

Looking for leptogluons

Dorival Gonçalves-Netto,^{1,2} David López-Val,¹ Kentarou Mawatari,³ Ioan Wigmore,⁴ and Tilman Plehn¹

¹*Institut für Theoretische Physik, Universität Heidelberg, Germany*

²*Max-Planck Institut für Physik, Munich, Germany*

³*Theoretische Natuurkunde and IIHE/ELEM, Vrije Universiteit Brussel, Belgium
and International Solvay Institutes, Brussels, Belgium*

⁴*SUPA, School of Physics & Astronomy, The University of Edinburgh, Scotland, UK*

We present search results based on next-to-leading order predictions for the pair production of color-adjoint leptons at the LHC. Quantum effects are sizable, dominated by pure QCD corrections, and sensitive to threshold effects. We illustrate the stabilization of scale dependences and confirm an excellent agreement between fixed-order and multi-jet predictions for representative distributions. Finally, we examine the trademark collider signatures of leptogluon pairs. Based on the CMS leptoquark search we derive a mass bound of 1.2-1.3 TeV for charged leptogluons, significantly improving the constraints available in the literature.

Contents

I. Introduction	2
II. Leptogluon pairs to NLO	2
A. Production rates	3
B. Real emission	5
C. Virtual corrections	5
D. Scale dependence	7
E. Distributions vs jet merging	8
III. Leptogluon signatures	9
A. Signal vs background	10
B. Data	12
IV. Summary	14
Acknowledgments	15
Appendix: renormalization	15
References	17

I. INTRODUCTION

Leptogluons are color-adjoint fermions with non-zero lepton number. We can categorize them as strongly interacting partners of the Standard Model leptons. Leptogluons may arise, for instance, as a manifestation of compositeness [1]. Proposals along these lines are motivated by the flavor and high-scale gauge structure of the Standard Model which suggests a relation between quarks and leptons. This can be explained, for instance, if both types of particles share a common substructure and emerge as bound states of fundamental constituents. These building blocks will be bound together by a new confining force. The onset of a confinement scale Λ will characterize the typical masses of the new heavy composites. If the basic quark and lepton constituents turn out to be charged under the Standard Model gauge group the new composite quarks and leptons will inherit these gauge charges and will thus be pair-produced through their ordinary couplings to gauge bosons. Alternatively, they can be produced in association with their Standard Model counterparts, via higher dimensional operators which govern the radiative transitions between both.

Historically, the seminal ideas on compositeness [3] crystallized into a paradigmatic class of models, the so-called preon models [4]. With the term *preon*, as coined by Pati and Salam, one denotes these more fundamental building blocks of Nature, whose condensates make up the “elementary” quarks and leptons, together with a tower of excited states. For example, in the framework of the so-called fermion-scalar models, the Standard Model leptons emerge as bound states from the combination of a fermionic preon and a scalar anti-preon $l \equiv (F\bar{S})$; if these constituents are charged under $SU(3)_c$, this naturally leads to leptonic composites of the sort $3 \otimes \bar{3} = 1 \oplus 8$: the color-singlet state can then be identified with an ordinary lepton, while the color-octet lepton corresponds to a leptogluon, e.g. the color-octet electron e_8^\pm . This argument illustrates how novel fermionic states transforming under higher $SU(3)_c$ representations serve as telltale predictions of compositeness models. Scalar or vector leptoquarks are another example of such heavy colored resonances [5]. More generally, TeV-scale strongly interacting sectors are typically linked to some kind of compositeness [6–9]. Their collider imprints, for instance the production of exotic objects such as e.g. excited leptons [10], quark sextets and decouplets [11], have been gathering attention in the recent years.

Phenomenological studies of leptogluon production are available for a diversity of frameworks, ranging from dedicated calculations of leptogluon pair production at e^+e^- , ep , and $pp(\bar{p})$ colliders [12] to generic approaches where the characteristic signatures of exotic colored states are portrayed, not only at colliders [11, 13] but also for precision physics [14]. Very recently, studies on the prospects of leptogluon searches at the LHC [15] and the LHeC [16] have been published.

Experimentally, the current 3σ , model-independent mass bounds from collider searches yield $m_{e_8} > 86$ GeV for a stable charged lepton octet; and $m_{\nu_8} > 110$ GeV, in the case of its neutral analogue ν_8 [17]. Dedicated analyses by JADE and H1 more than two decades ago have extracted leptogluon mass bounds attached to specific compositeness scale choices, typically in the range of $m_{e_8^\pm} \sim 100 - 200$ GeV for $\Lambda \sim 1 - 2$ TeV [18].

In this paper we analyse the production of leptogluon pairs to next-to-leading order (NLO) QCD. We compute the total leptogluon pair production rates and examine in detail the different quantum effects. The reduced theoretical uncertainties we illustrate via the stabilization of the NLO predictions with respect to variations of the (unphysical) renormalization and factorization scales. We compute representative kinematic distributions to NLO and compare them to independent results based on multi-jet merging. All these NLO calculations we carry out with the help of the fully automated package MADGOLEM [19–22]. Finally, we explore the characteristic collider signatures of leptogluon pair production and discuss the prospects for leptogluon searches at the LHC.

II. LEPTOGLUON PAIRS TO NLO

We analyse the phenomenology of leptogluons at the LHC assuming a minimal extension of the Standard Model. We entertain the existence of an additional generation of lepton octets which consists of one electrically charged, color-adjoint (Dirac) lepton — the *electron/positron octet* e_8^\pm — and its neutral companion, a *neutrino octet* ν_8 . Generically, we shall label these fields as $l_8 \equiv e_8^\pm, \nu_8$. For our analysis, no assumption needs to be made on their possible weak charges. For concreteness, and unless otherwise stated, we shall assume both states to be mass degenerate. This setup provides a minimal, but representative framework in which to explore the trademark collider imprints of leptogluons. Interestingly, neutrino octets from compositeness scenarios and gluino fields from supersymmetric models share the same quantum numbers (barring the lepton number). In this sense, neutrino octets will portray very similar aspects as gluinos, with no connection to the supersymmetric nature of the latter.

Leptogluon interactions at the LHC are entirely driven by QCD. As $SU(3)_c$ adjoints leptogluons couple to gluons through the covariant derivative $(D_\mu)_{AB} = (\partial_\mu)_{AB} + i g_s (T^C A_\mu^C)_{AB}$, where A_μ^C denotes the gluon field, g_s the

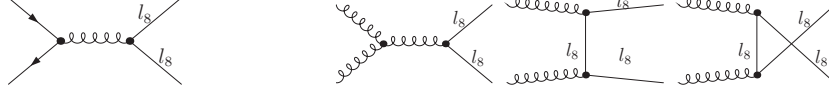


Figure 1: Feynman diagrams for the pair production of leptogluons to leading order. We represent both partonic subprocesses: quark-antiquark annihilation $q\bar{q} \rightarrow l_s \bar{l}_s$ and gluon fusion $gg \rightarrow l_s \bar{l}_s$.

strong coupling constant, and T^C the adjoint $SU(3)_c$ generators. We write these generators in terms of the structure constants $T_{BC}^A = -if^{ABC}$. The Lagrangian that describes the gl_sl_s coupling then yields

$$\mathcal{L} \supset \bar{\psi}_{l_s} (i\not{D} - m_{l_s}) \psi_{l_s} \supset -g_s f^{ABC} \bar{\psi}_{l_s}^A \gamma^\mu \psi_{l_s}^B A_\mu^C. \quad (1)$$

There are two partonic subprocesses which contribute to pair production of leptogluons at the LHC: quark-antiquark annihilation and gluon fusion (cf. Figure 1):

$$pp(q\bar{q}) \rightarrow l_s \bar{l}_s \quad \text{and} \quad pp(gg) \rightarrow l_s \bar{l}_s, \quad (2)$$

where $l_s \bar{l}_s$ can either stand for the production of a charged $e_s^- e_s^+$ or a neutral $\nu_s \nu_s$ leptogluon pair. Throughout our analysis we set the central renormalization and factorization scales to the average final state mass $\mu^0 \equiv \mu_{R,F} = m_{l_s}$, which leads to stable perturbative results [23, 24]. Unless stated otherwise, we fix the LHC energy to $\sqrt{S} = 8$ TeV, while the default leptogluon mass choice is $m_{l_s} = 1$ TeV. As for the parton densities we use CTEQ6L1 and CTEQ6M [25] with five active flavors. The corresponding values for the strong coupling constant α_s are computed with consistent values of $\alpha_s(\mu_R)$ obtained via two-loop running from Λ_{QCD} to the required renormalization scale μ_R , again in the five active flavor scheme.

A. Production rates

We first concentrate on the total cross section for leptogluon pair production, $\sigma(pp \rightarrow l_s \bar{l}_s)$, computed to leading and next-to-leading order with the associated K factors. A comprehensive numerical survey we document in Table I. We consider leptogluon masses ranging from 500 GeV to 1.5 TeV. From here on we shall concentrate on the production of electron-octet pairs, $pp \rightarrow e_s^+ e_s^-$. The neutrino octet field ν_s only contributes as a new colored virtual particle, entailing a mass-suppressed and hence numerically mild contribution. The constant ratio

$$\frac{\sigma(pp \rightarrow e_s^+ e_s^-)}{\sigma(pp \rightarrow \nu_s \nu_s)} = 2 \quad (3)$$

reflects the fact that, so long as $m_{e_s^\pm} = m_{\nu_s}$, the differences between the charged and the neutral channels reduce to a symmetry factor 1/2, which accounts for the two identical particles in the $\nu_s \nu_s$ final state. The results we present for three LHC nominal energies: $\sqrt{S} = 7, 8, 14$ TeV.

The total cross sections are sizable and very strongly dependent on the leptogluon mass. Leptogluons with $m_{l_s} \sim 500$ GeV would be typically produced at a rate of 1 – 10 pb. TeV-scale leptogluons, in turn, range around $\mathcal{O}(10)$ fb.

$pp \rightarrow e_s^+ e_s^-$ m_{l_s} [GeV]	$\sqrt{S} = 7$ TeV			$\sqrt{S} = 8$ TeV			$\sqrt{S} = 14$ TeV		
	σ^{LO} [pb]	σ^{NLO} [pb]	K	σ^{LO} [pb]	σ^{NLO} [pb]	K	σ^{LO} [pb]	σ^{NLO} [pb]	K
500	2.39×10^0	4.77×10^0	2.00	4.35×10^0	8.61×10^0	1.98	3.84×10^1	6.84×10^1	1.78
700	1.86×10^{-1}	3.84×10^{-1}	2.06	3.85×10^{-1}	7.89×10^{-1}	2.05	4.98×10^0	9.08×10^0	1.83
900	2.13×10^{-2}	4.42×10^{-2}	2.08	5.02×10^{-2}	1.04×10^{-1}	2.08	9.20×10^{-1}	1.76×10^0	1.91
1100	2.88×10^{-3}	6.03×10^{-3}	2.09	8.04×10^{-3}	1.68×10^{-2}	2.09	2.20×10^{-1}	4.26×10^{-1}	1.94
1300	4.08×10^{-4}	8.86×10^{-4}	2.17	1.43×10^{-3}	3.03×10^{-3}	2.12	6.21×10^{-2}	1.21×10^{-1}	1.95
1500	6.00×10^{-5}	1.36×10^{-4}	2.27	2.64×10^{-4}	5.73×10^{-4}	2.17	1.94×10^{-2}	3.82×10^{-2}	1.97

Table I: Total cross sections $\sigma(pp \rightarrow e_s^+ e_s^-)$ and corresponding K factors, for different leptogluon masses and LHC energies. The renormalization and factorization scales we fix to the central value $\mu_R = \mu_F = \mu^0 = m_{l_s}$.

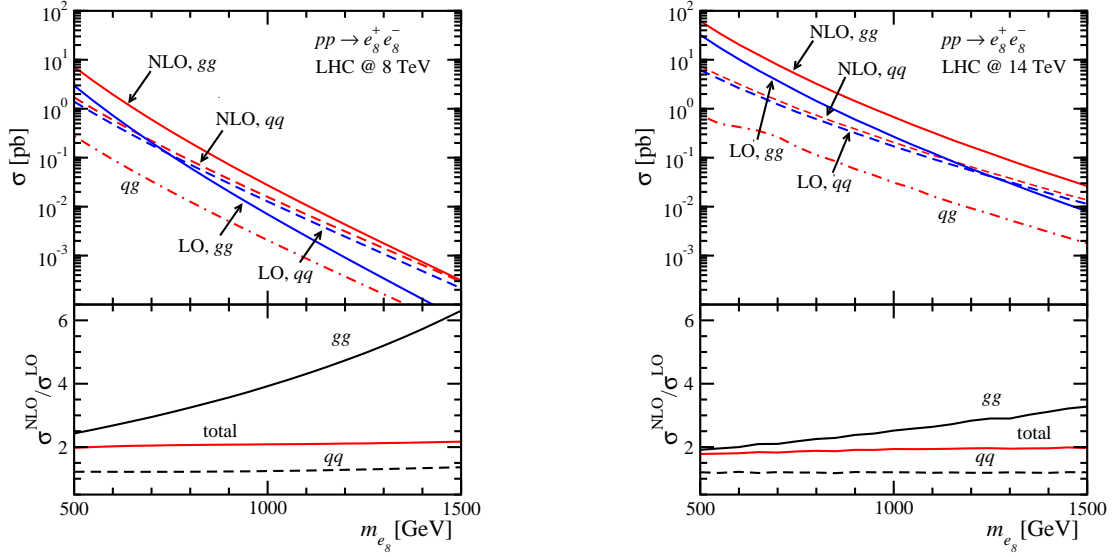


Figure 2: LO and NLO contributions from the gg and $q\bar{q}$ partonic subchannels to the total rates (above) and K factor (below) for leptogluon pair production $\sigma(pp \rightarrow e_s^+ e_s^-)$. The center-of-mass energy we fix at 8 (left panel) and 14 TeV (right).

The size of the QCD quantum effects we quantify as $K \equiv \sigma^{\text{NLO}}/\sigma^{\text{LO}}$. This may attain very large values, spanning the range of 1.8 to 2.0 for $\sqrt{S} = 14$ TeV, or even higher values 2.0-2.2 for $\sqrt{S} = 8$ TeV. These uncomfortably large K -factors we should not interpret as a breakdown of perturbation theory. Instead, they signal artificially low LO production rates for $\mathcal{O}(1)$ TeV mass particles, a known problem of the CTEQ parton densities [21, 22]. The NLO cross sections are actually perturbatively stable. On the other hand, the growth of the K -factors as the leptogluon mass increases we can trace back in part to a non-trivial threshold behavior from the real and the virtual NLO contributions, which partially overcomes the phase space suppression of the NLO contributions. We will expand on all these aspects below.

The total rates drop nearly three orders of magnitude when sweeping the leptogluon mass range from 0.5 to 1.5 TeV. A closer view into this mass dependence we display in Figure 2. Herewith we profile the cross section (top panel) and K -factor (down panel) as a function of $m_{e_s^\pm}$ for the different partonic subchannels. The LHC energy we fix to 8 TeV (left) and 14 TeV (right). The dominance of the gg -initiated mechanism for low-mass leptogluons — roughly one order of magnitude above $q\bar{q}$ — follows from the large gluon luminosity; for larger m_{l_s} values this effect is inverted. The $q\bar{q}$ mechanism includes not only the contribution from the valence quarks u, d but also the suppressed flavor excitations from the second generation, which amount to less than 10% of the $q\bar{q} \rightarrow e_s^+ e_s^-$ budget. The quark-gluon crossed channels qg , which arise purely at NLO, stagnate at the per-mil level given our treatment of the collinear divergences [22].

In more detail, we can read off Figure 2 that $\sigma(gg \rightarrow l_s \bar{l}_s)$ to LO depletes faster than $\sigma(q\bar{q} \rightarrow l_s \bar{l}_s)$ with increasing leptogluon masses, *i.e.* the associated K factor K_{gg} exhibits a steeper growth. Unsurprisingly, we encounter a similar behaviour for gluino pairs [26]. These features we can understand, on the one hand, from the scaling at threshold, as we will explain in detail later. Moreover, they can again be related to the respective parton luminosities. Heavy leptogluon masses probe larger values of the Bjorken x -variable — this being the region where the quark parton densities become more competitive as compared to the gluon ones.

It is illustrative to compare the leptogluon production rates to similar QCD-driven heavy particle production, in particular squarks [22–24], gluinos [22, 26], and sgluons [21]. Based on MADGOLEM [19] and PROSPINO [23, 24] we can establish the hierarchy

$$\sigma(pp \rightarrow l_s \bar{l}_s) \sim \sigma(pp \rightarrow \tilde{g}\tilde{g}) \sim \mathcal{O}(10) \times \sigma(pp \rightarrow GG^*) \sim \mathcal{O}(100) \times \sigma(pp \rightarrow \tilde{q}\tilde{q}^*). \quad (4)$$

The differences we may track down to larger color charges involved in the production of color-adjoints as compared to fundamentals and to the spin representation of the final-state particles. The production of fermion pairs like leptogluons and gluinos is more efficient than that of sgluons. Finally, it is also worth pointing out that the phenomenological profile of leptogluon and leptoquark pair production is very similar, in spite of their different spin and color representations. We will further exploit these coincidences in Section III.

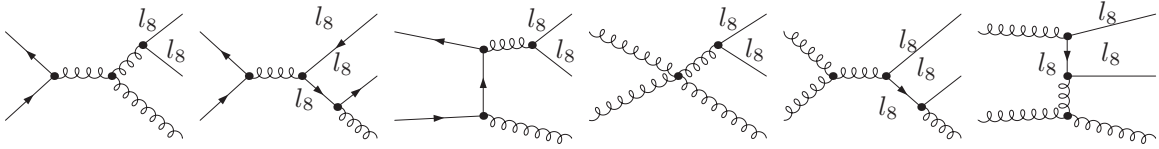


Figure 3: Sample Feynman diagrams describing the real emission corrections for the pair production of leptogluons via quark-antiquark annihilation (left) and gluon fusion (right).

B. Real emission

Real emission is part of the QCD quantum effects to leptogluon pair production. It comprises the $\mathcal{O}(\alpha_s^3)$ three-particle final states with a leptogluon pair plus an additional parton, which accounts for the QCD jet radiation, either from the initial-state partons or the final-state leptogluons (cf. Figure 3).

These contributions are infrared divergent, as a result of the soft and collinear singularities developed by the initial-state radiation, as well as the soft poles from the gluon radiation off the leptogluon legs. These infrared divergences we subtract using massive Catani-Seymour dipoles [27, 28]. On top of the Standard Model initial-initial and initial-final dipoles MADGOLEM automatically provides the corresponding leptogluon dipoles which are required for new final-final and final-initial singularities. Since the leptogluons are color octet massive fermions, their dipoles are equivalent to the massive fermions with the replacement of the color factors $C_F \rightarrow C_A$.

The MADGOLEM implementation is based on an extended version of MADDIPOLE [29] and retains a variable phase space coverage in terms of the FKS-style cutoff $0 < \alpha \leq 1$ [30]. As the default value we use $\alpha = 1$. The numerical performance of the leptogluon dipole we can assess from Figure 4. Notice that while the individual contributions from the integrated and the non-integrated dipoles diverge logarithmically for small α their sum is stable over roughly eight orders of magnitude. These results we compute for the $u\bar{u} \rightarrow e_s^+ e_s^- g$ partonic subprocesses, assuming 1 TeV leptogluon final states.

C. Virtual corrections

The second class of NLO quantum effects includes $\mathcal{O}(\alpha_s^3)$ terms from the exchange of virtual gluons, quarks and leptogluons, giving rise to self-energy, vertex and box one-loop corrections. A sample of the corresponding Feynman diagrams we display in Figure 5. Again, we compute them using MADGOLEM [19], generating the one-loop amplitudes with QGRAF[31]. To handle the helicity and color structures we rely on a dedicated set of currently in-house routines, prior to finally reducing their tensor structures in the GOLEM [32, 33] framework. The resulting one-loop integrals we numerically evaluate with the ONELOOP library [34]. For a detailed account on the structure and performance of the tool, we refer the reader to Ref. [19].

All divergences we regularize using standard dimensional regularization, analytically extending all integrals and internal propagators to $n = 4 - 2\epsilon$ dimensions. We then subtract the infrared poles by including the integrated Catani-Seymour dipoles. The collinear higher-order corrections we absorb into the parton densities. The ultraviolet

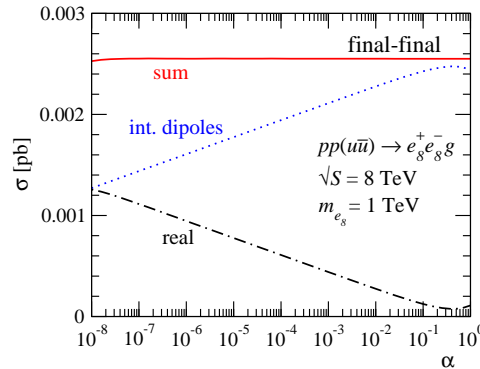


Figure 4: Dependence on the FKS-like α parameter corresponding to the final-final leptogluon Catani-Seymour dipole for the partonic subchannel $u\bar{u} \rightarrow e_s^+ e_s^- g$. The leptogluon mass we fix at $m_{e_s} = 1 \text{ TeV}$.

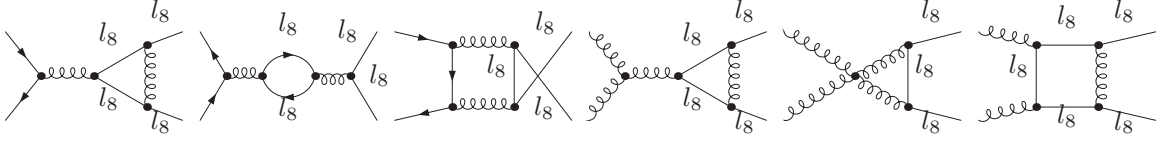


Figure 5: Sample Feynman diagrams describing the NLO virtual corrections to the pair production of leptogluons via quark-antiquark annihilation (left) and gluon fusion (right).

divergences in turn cancel against the corresponding ultraviolet counter terms, which are part of the *leptogluon_nlo* model implementation and are generated automatically. Its structure is completely defined by the on-shell renormalization of the leptogluon mass and the $\overline{\text{MS}}$ renormalization of the strong coupling constant, with a decoupling of the heavy colored degrees of freedom [35]. We check the cancellation of divergences both analytically and numerically. The finite parts for the one-loop amplitude we compare to an independent implementation of the leptogluon model in FEYNARTS, FORMCALC and LOOPTOOLS [36]. In the Appendix we supply further details on the renormalization.

We examine in detail the anatomy of the virtual corrections in Figures 6-7. The patterns share many common features with sgluon [21] and gluino [22, 26] pair production. To start with, in Figure 6 we survey the mass dependence of the real and the virtual corrections for both parton channels gg and $q\bar{q}$. For each of them we superimpose the total LO and NLO rates, together with the partial NLO virtual and real contributions σ^{virtual} and σ^{real} (upper panels), while the relative size of the NLO corrections we depict below.

The different subsets of one-loop topologies we examine in Figure 7. Their relative weight with respect to the LO results we describe via the ratio $\Delta\sigma/\sigma^{\text{LO}} \equiv (\sigma^{\text{NLO},i} - \sigma^{\text{LO}})/\sigma^{\text{LO}}$, where i runs over all the different one-loop contributions — including gluon emission which enters through the integrated dipoles. Again, we separate the gg and $q\bar{q}$ subchannels. The crossed channel qg does not develop any virtual corrections and hence it is not included. Notice, though, that it is required to achieve a complete cancellation of the collinear divergences. The figure unveils, first of all, large vertex corrections to the QCD coupling $ge_8^+e_8^-$ of at least $\mathcal{O}(40\%)$ and with opposite signs for each of the subchannels. The corresponding mass dependence turns out to be relatively mild, with a total variation not larger than $\sim 10\%$ for the whole leptogluon mass range under scrutiny.

Sizable (positive) corrections are driven by the integrated Catani–Seymour dipoles, i.e. from soft/collinear gluon emission. Also large are the box contributions for the gg initial state. Finally, leptogluon self-energy corrections become large for the gg initial state. Interestingly, they all feature a characteristic growth with the leptogluon mass. Both, the size and the acute mass dependence of these subsets we can trace back to genuine kinematical and dynamical features.

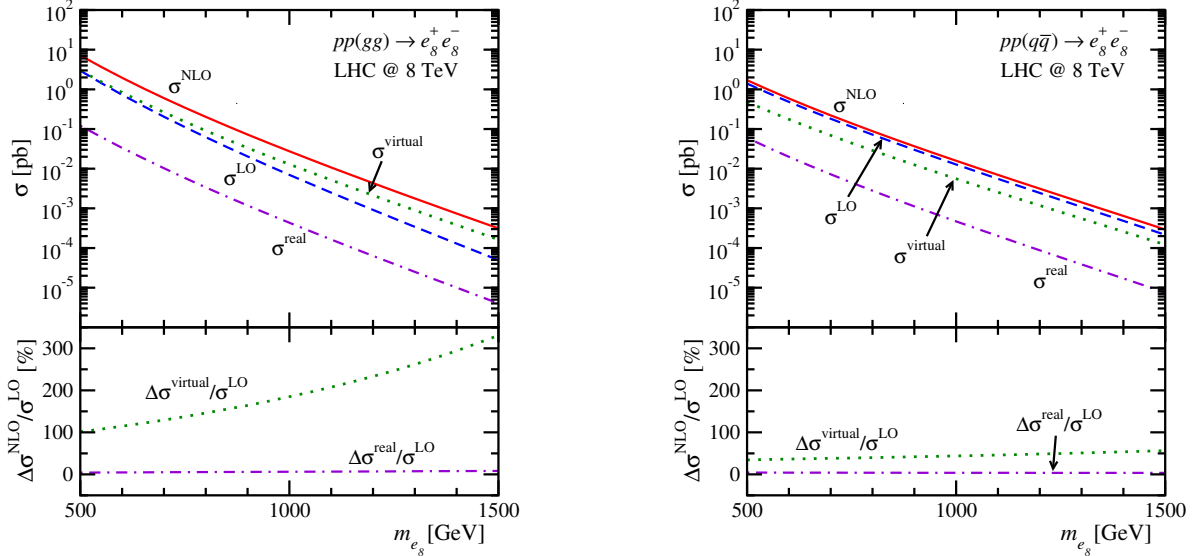


Figure 6: Total LO and NLO leptogluon pair cross sections $\sigma(pp \rightarrow e_8^+ e_8^-)$ as a function of the mass. We separate gluon fusion (left) and quark/antiquark annihilation (right). In the lower panels we account for the relative size of the corrections, separated using Catani–Seymour dipoles with $\alpha = 1$ and including the integrated dipoles as part of the virtual contribution.

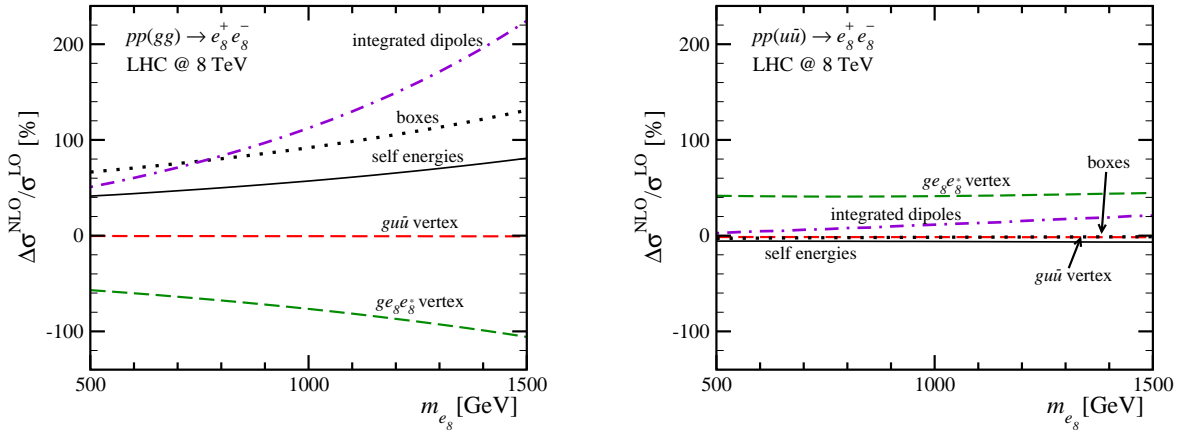


Figure 7: Relative size $\Delta\sigma^{\text{NLO}}/\sigma^{\text{LO}} \equiv (\sigma^{\text{NLO}} - \sigma^{\text{LO}})/\sigma^{\text{LO}}$ for the different one-loop contributions as a function of the leptogluon mass. The two leading-order parton channels $\sigma(gg \rightarrow l_s l_s)$ (left) and $\sigma(u\bar{u} \rightarrow l_s l_s)$ (right) we show separately. The integrated dipoles we show for $\alpha = 1$.

The steeper growth of the K factors for the gg -initiated subprocess can be in part understood from the LO threshold behavior: there, the rate scales like $\sigma_{gg} \sim \pi m_{l_s}^2/\hat{S}$ versus $\sigma_{q\bar{q}} \sim \pi m_{l_s}^2\beta/\hat{S}$, with $\beta^2 = 1 - 4m_{l_s}^2/\hat{S}$, which means that $\sigma^{\text{LO}}(gg \rightarrow l_s l_s)$ decreases faster than $\sigma^{\text{LO}}(q\bar{q} \rightarrow l_s l_s)$ with growing leptogluon mass. The dominant virtual corrections benefit from two threshold effects. An enhanced Sommerfeld rescattering [37] describes the exchange of soft gluons between slowly-moving final-state leptogluons, leading to a Coulomb singularity $\sigma^{\text{virtual}} \sim \pi\alpha_s/\beta$. The complete logarithmic enhancement of the soft gluon emission behaves like $\sigma \sim A \log^2(\beta) + B \log(8\beta^2)$.

Both sources of threshold enhancements become more efficient close to threshold for the steep gluon luminosities and at large leptogluon masses, and can eventually be resummed [38].

The enhanced leptogluon self energies in the $gg \rightarrow l_s \bar{l}_s$ case can be correlated to the leptogluon mass insertion in the t and u -channel leptogluon exchange – with no counterpart for $q\bar{q} \rightarrow l_s l_s$. The remaining one-loop contributions, consisting of QCD-like quark-gluon and triple-gluon vertex corrections and the box and self-energy corrections for $q\bar{q} \rightarrow l_s l_s$ are essentially featureless and contribute with overall yields below 10%.

D. Scale dependence

One of the main motivations of higher-order predictions is to stabilize the (unphysical) dependence on the renormalization and factorization scales. We introduce them when we remove the collinear and ultraviolet divergences at a given order in the perturbative series. In the limit where all terms in such series are retained the scale dependence

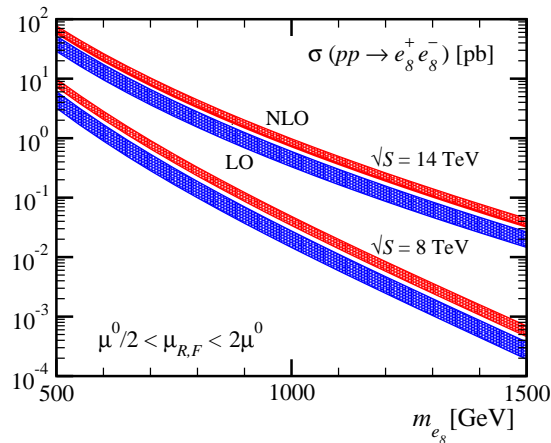


Figure 8: Leptogluon pair cross section $\sigma(pp \rightarrow e_s^+ e_s^-)$ as a function of the leptogluon mass. The scale uncertainty envelope corresponds to an independent renormalization and factorization scale variation in the range $\mu^0/2 < \mu_{R,F} < 2\mu^0$.

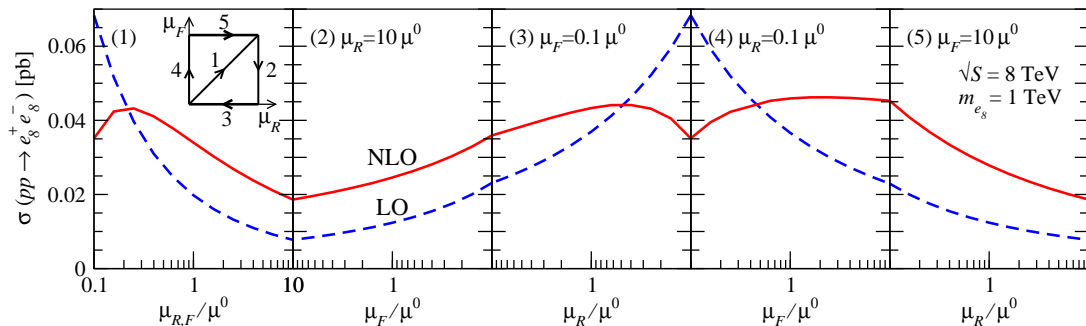


Figure 9: Renormalization and factorization scale dependence for leptogluon pair production $pp \rightarrow e_s^+ e_s^-$. The plots trace a contour in the μ_R - μ_F plane in the range $\mu = (0.1 - 10) \times \mu^0$ with $\mu^0 = m_{e_s^\pm}$, and $m_{e_s^\pm} = 1$ TeV.

vanishes. In practice, we truncate the expansion on the coupling constant at a certain order $\mathcal{O}(\alpha_s^n)$. In the absence of any systematic correlation between different orders n we expect the scale dependence to englobe the asymptotic cross-section values. This expectation has been well confirmed for many QCD-mediated processes [21–24].

In Figure 8 we depict the evolution of the total leptogluon pair cross sections at LO and NLO with the leptogluon mass, for the LHC operating at 8 and 14 TeV. The band envelope accounts for the theoretical uncertainty, which we estimate as conventionally by varying the scale choices within the range $\mu^0/2 < \mu_{R,F} < 2\mu^0$. We see that over the entire mass range the LO and NLO curves hardly overlap, which means that at least for the LO cross section a scale variation by a factor two around the central scale would not have been a conservative estimate of the theory uncertainty due to missing higher orders in perturbation theory.

Complementary vistas on the stabilization of the scale dependence we provide in Figure 9. We delineate the LO and NLO cross sections for an independent variation of the factorization and renormalization scales. The five panels correspond to a contour in the $\mu_R - \mu_F$ plane, which we define in the left panel. The smoothing of $\sigma(\mu)$ at NLO nicely illustrates the stabilization of the higher order prediction with respect to scale choices. Quantitatively, the LO variation stays within $\Delta\sigma^{\text{LO}}/\sigma^{\text{LO}} \sim \mathcal{O}(65\%)$, while at NLO it reduces to $\Delta\sigma^{\text{NLO}}/\sigma^{\text{NLO}} \sim \mathcal{O}(30\%)$.

E. Distributions vs jet merging

Relying on fixed order NLO predictions we can extract a suitable normalization to the event rates from standard Monte Carlo simulations. Nevertheless, one still needs to assure that this framework can be safely promoted to the main distributions. It has been shown in the literature that transverse momentum and rapidity distributions are relatively stable with respect to higher order corrections for heavy particle production [20–23]. As long as the collinear approximation includes sizable p_T values owing to even larger final-state masses QCD jet radiation should be properly accounted for by the parton shower description [21, 39, 40].

In Figure 10 we check these expectations. Therewith, we display the transverse momentum and rapidity distributions for 1 TeV leptogluons. The different LO and NLO pieces we display separately. Real emission and virtual NLO effects we disentangle by introducing Catani–Seymour dipoles and separating the corresponding phase space regions within $\alpha = 10^{-3}$. We can then compare the fixed-order NLO results from MADGOLEM with a matched matrix element and parton shower description using the MLM scheme including up to two hard jets [41, 42]. For the latter we employ MADGRAPH5 [40, 43] interfaced with PYTHIA [44]. We explicitly check that including just one hard jet barely changes the results, in line with the general statement that in our case the collinear parton shower is not a bad approximation.

The two main histograms we normalize to unity, with the different NLO contributions shown to scale. Both approaches display very similar shapes, featuring central leptogluons with transverse momentum peaking at $p_T(e_s^\pm) \simeq 300$ GeV. Only when analysed individually, the p_T curves for the real and virtual NLO corrections depart significantly from the combined curve. The observed shift towards slightly harder and more central leptogluons in the merged result, which also appears for sgluon pairs [21], we can deem to the additional recoil jets.

Finally, in Figure 11 we present a panoply of Figure 10, now displaying the transverse momentum and rapidity dependence of the K -factors including the scale dependence envelope around the central scale $\mu^0 = m_{e_s^\pm}$. Remarkably, the K -factors remain relatively constant within the remaining NLO scale dependence as long as we stay within central rapidities and p_T values around $m_{e_s^\pm}/2 \gtrsim 500$ GeV. This justifies the use of the K -factor as an overall reweighting

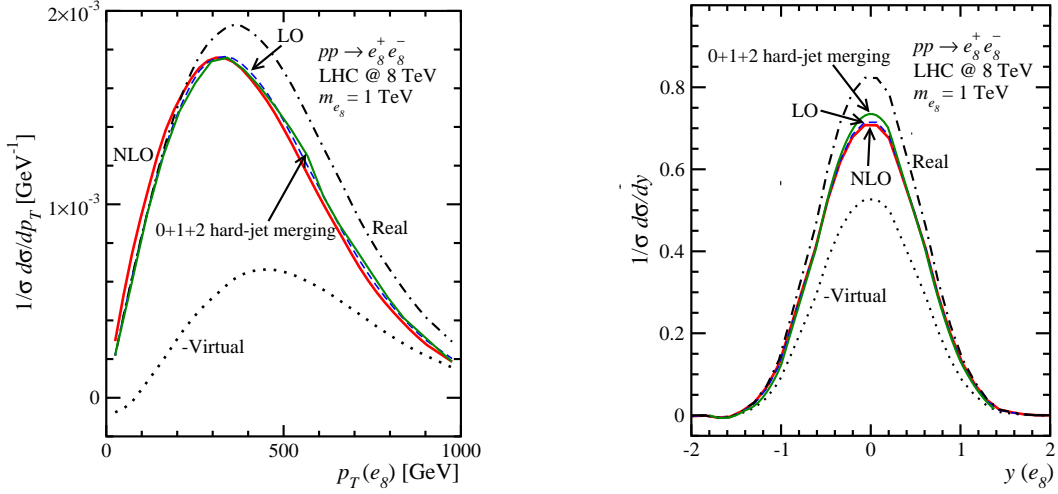


Figure 10: NLO distributions for leptogluon pair production as a function of the transverse momentum $p_T(e_g^\pm)$ and rapidity $y(e_g^\pm)$. For the NLO curves we separately display the LO, virtual, and real contributions, separated using Catani–Seymour dipoles with $\alpha = 10^{-3}$. In addition, we show the distributions based on LO matched samples with up to two hard jets. The NLO and matched curves we normalize to unity while the different contributions to the NLO rates we show to scale.

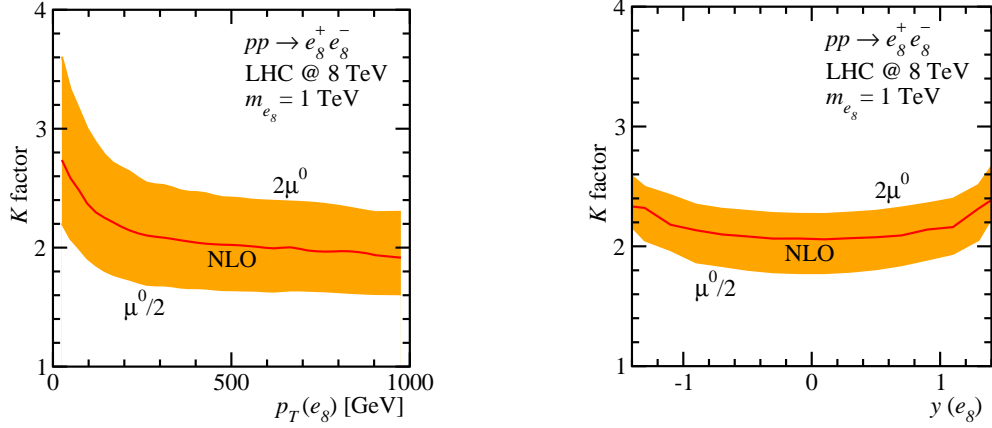


Figure 11: K factor as a function of the leptogluon transverse momentum $p_T(e_g^\pm)$ and rapidity $y(e_g^\pm)$. We include the scale uncertainty envelope for an independent renormalization and factorization scale variation within $\mu^0/2 < \mu_{R,F} < 2\mu^0$.

factor for the leading-order event samples as long as we do not probe extreme phase space regions – see *e.g.* [45] for a counter example.

III. LEPTOGLUON SIGNATURES

From here on we will focus on trademark collider signatures of leptogluon pairs and discuss them in the light of the current LHC searches. Specifically, we discuss how to make use of ongoing CMS searches for leptoquarks [46] to provide updated leptogluon mass bounds.

Besides the $SU(3)_c$ gauge couplings leptogluons can also interact with matter fields. These interactions are ultimately induced by the dynamics of the underlying model. They appear as non-renormalizable couplings which we can parameterize through higher dimensional effective operators. For simplicity, we limit ourselves to the dimension-5 chromomagnetic operator. It is a representative example of such non-renormalizable couplings and accounts for the radiative decay of a leptogluon decay into a lepton and a gluon. This process is governed by the effective Lagrangian

$$\mathcal{L} = \frac{g_s}{2\Lambda} \bar{\psi}_{l_s}^A \sigma^{\mu\nu} G_{\mu\nu}^A (a_L P_L + a_R P_R) \psi_l + \text{h.c.} , \quad (5)$$

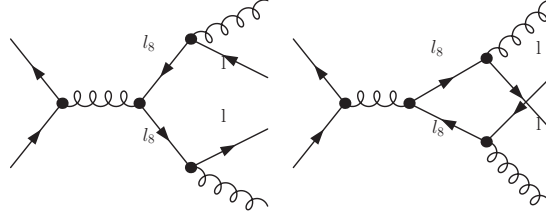


Figure 12: Sample Feynman diagrams describing the characteristic dijet–dilepton final-state from leptogluon pair production followed by a radiative transition into a Standard Model lepton and a gluon each.

with Λ denoting the characteristic scale of the ultraviolet completion, e.g. the compositeness scale of a hypothetical preonic model. The spinors $\psi_{l_s}^A$ and ψ_l describe the leptogluon and Standard Model lepton. In the presence of the gluon we factorize the strong coupling constant g_s . The overall coupling strength is affected by the parameters $a_{L/R}$ which we expect to be of $\mathcal{O}(1)$. If instead of a strongly-interacting ultraviolet completion this transition is mediated by quantum effects we expect another suppression factor $1/16\pi^2$. Henceforth, we assume $a_R = 0$, in agreement with electron chirality conservation and the left-handed nature of the Standard Model neutrinos.

In the decay of leptogluons into a Standard Model lepton and a gluon both (massless) daughter particles emerge as back-to-back hard objects in the leptogluon rest frame. The leptogluon partial width we compute from the effective Lagrangian Eq.(5), and we may cast it into the following form

$$\Gamma_{l_s \rightarrow lq} = \frac{g_s^2 m_{l_s}^3}{16\pi\Lambda^2} (a_L^2 + a_R^2). \quad (6)$$

This form coincides with the width of a gluino decaying into a gravitino-gluon final state [47] after matching the respective effective couplings. Such analogies between leptogluons and gluinos are also rubber-stamped into their respective collider footprints, cf. Ref [48] for a detailed account on associated gluino-gravitino production at the LHC.

We show a sample of leading-order Feynman diagrams for the pair production of leptogluons and their subsequent radiative decay in Figure 12. The overall rates we can describe within the narrow width approximation,

$$\sigma(pp \rightarrow l_s \bar{l}_s \rightarrow llgg) \simeq \sigma(pp \rightarrow l_s \bar{l}_s) \times [\text{BR}(l_s \rightarrow lg)]^2. \quad (7)$$

The narrow width approximation is manifest from Eq.(6) and assuming $a_{L(R)}^2/\Lambda^2 \ll 1$. As a consequence the leptogluon signatures will essentially not depend on the effective higher-dimensional interactions modelling the leptogluon decay. We should be able to derive universal constraints on the leptogluon masses unrelated to the characteristic ultraviolet scale Λ and the coupling strength $a_{L(R)}$ of the effective $l_s lg$ interactions.

As already mentioned, searches for (charged) leptogluons at the LHC should close follow searches for leptoquarks, as both processes share the same final-state signature [46]. It consists of two isolated hard leptons alongside two central jets. These leptons get replaced by neutrinos or missing energy when we instead entertain the case of neutral leptogluons. As heavy resonances, leptogluon decays naturally give rise to hard p_T profiles for the resulting products, as well as sizable invariant masses for the dilepton $m(e^+e^-)$ and leading- p_T dijet systems $m(jj)$. Irreducible Standard Model backgrounds are $Z/\gamma^*/W$ +jets, W^+W^- +jets, and $t\bar{t}$ production. Additional subleading sources are single top production, electroweak dibosons, and QCD multijets, typically well below the per-cent level.

A. Signal vs background

The signal and backgrounds in this section we simulate with MADGRAPH5 [43]. A minimal extension of the Standard Model including the leptogluon fields and corresponding interactions we implement via FEYNRULES [49], which also provides the corresponding UFO model files [50]. We use MADANALYSIS5 [51] to analyse the event samples. The effective coupling/scale ratio a_L/Λ we fix to 10^{-5} , with $a_R = 0$. While this choice has barely any impact on the total $\mathcal{O}(\alpha_s)$ leptogluon rates it suppresses additional $\mathcal{O}(\alpha_s a_{L/R}^2/\Lambda^2)$ channels from gluon fusion and a t -channel leptogluon exchange. For the leptogluon mass the default value is $m_{l_s} = 1$ TeV. For the LHC energy we assume $\sqrt{S} = 7$ TeV. The leptogluon effective couplings are diagonal in generation space, such that we search for electrons and electron-neutrinos, $l \equiv e^\pm, \nu_e$.

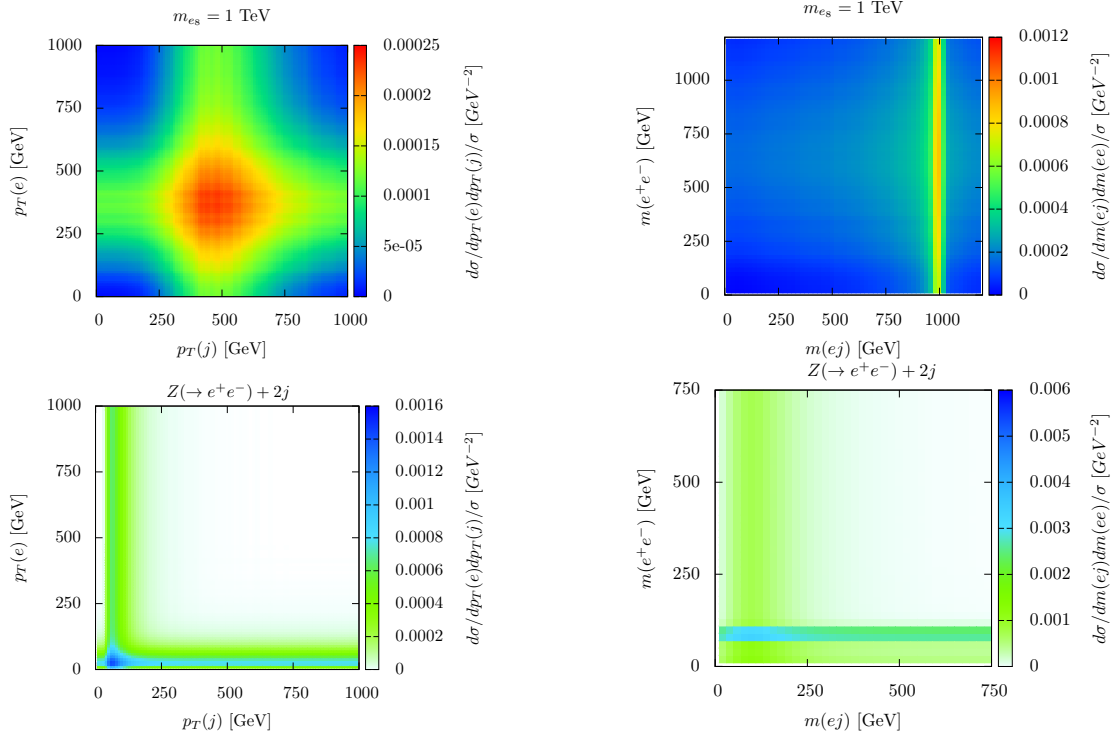


Figure 13: Correlated distributions for charged leptogluon pair production giving rise to $2j+2l$ final-states (top panels) and the leading Standard Model background $pp \rightarrow Z + \text{jets}$ (bottom panels). We explore the correlations between the hardest lepton and jet transverse momenta (left) and the invariant masses of the dilepton and the hardest jet-lepton systems (right).

As this process involves the production of colored heavy fields, we expect a sizable influence from the initial and final-state QCD radiation. This gives rise to multi-jet configurations which depart from the mere LO expectations and leave us with the separation of jets into QCD radiation and decay jets [21, 40, 45, 52]. We model QCD jet radiation using MLM jet merging as implemented in MADGRAPH5 to generate signal samples including up to two extra hard jets. Technically, we enforce $m_{ll}^{\min} = m_{jj}^{\min} = 10$ GeV, to avoid phase space singularities in the backgrounds.

Representative signal and background correlations between different distributions involving the hardest lepton and jet decay products we examine in Figure 13. They nicely illustrate the relevant kinematical features which we can rely on for a suitable search strategy. A first telltale imprint of the charged leptogluons involves hard charged leptons, each of them stemming from the decay of one of the leptogluons. This translates into very large dilepton $m(e^+e^-)$ and dijet $m(j_1j_2)$ invariant masses. The natural scale for the signal selection is $m(e^+e^-) \gtrsim m_Z$. The leptogluon mass reconstruction, in turn, should proceed through the lepton-jet invariant mass $m(ej)$ which we also display in Figure 13. Another hallmark involves the transverse momenta of the hardest jet and the outgoing charged leptons. Additional jet emission from the parton shower is responsible for a smearing of this peak. Since this feature is correlated with the leptogluon mass it will depart very visibly from the background structure, as shown in the bottom-left panel of Figure 13.

In analogy to the charged leptogluon case we show the relevant correlated distributions for the neutral leptogluon signal $pp \rightarrow \nu_8 \nu_8 \rightarrow \cancel{E}_T + \text{jets}$ in Figure 14. In the absence of identified leptons the experimental prospects are more challenging. After using a lepton veto to suppress the $t\bar{t}$ and $(Z/\gamma^* \rightarrow e^+e^-) + \text{jets}$ backgrounds the leading irreducible background is $Z + \text{jets}$ production with an invisible decay $Z \rightarrow \nu\nu$. The key observable is missing transverse energy \cancel{E}_T . The expected \cancel{E}_T from $Z + \text{jets}$ production displays a much softer profile than the signal. We illustrate these features in Figure 14.

More generally, signal and backgrounds substantially deviate from each other in the number of final-state jets. Owing to the $SU(3)_c$ adjoint charge of the leptogluons as well as to their large masses we expect the leptogluon events to yield larger jet multiplicities, as reflected in Figure 15. By the same token, we also retrieve a much harder total visible energy $H_T \equiv \sum_j p_T^j + p_T(e^+) + p_T(e^-)$, whose peak follows once more the leptogluon mass.

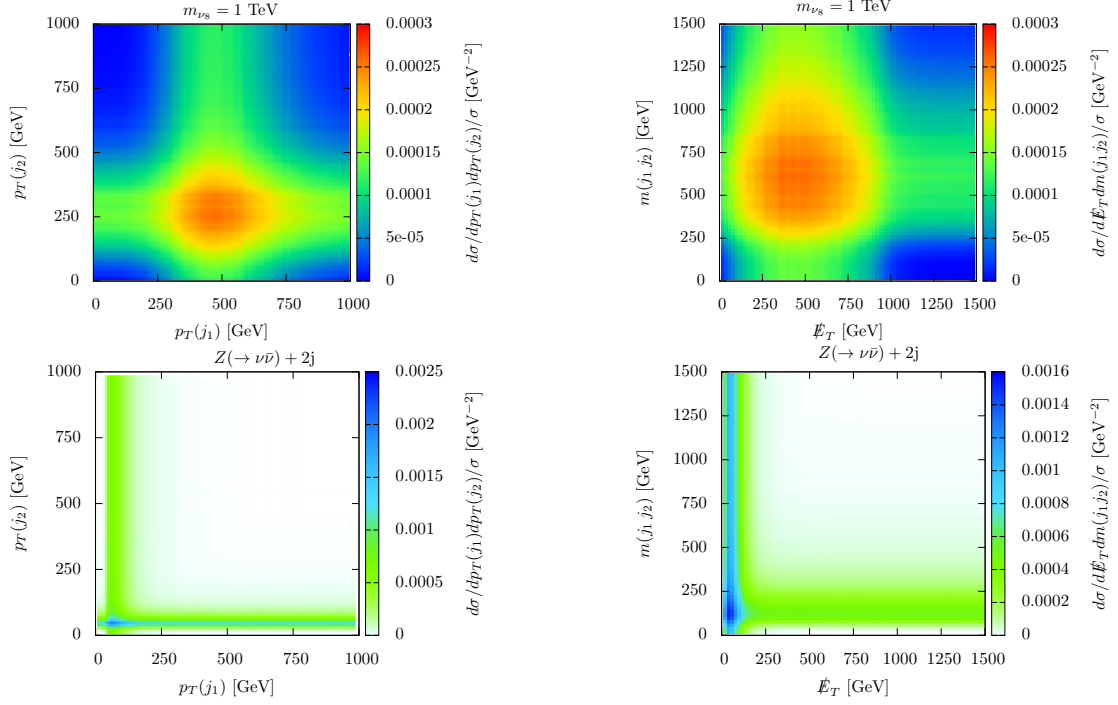


Figure 14: Correlated distributions for neutral leptogluon pair production giving rise to $2j + \cancel{E}_T$ final-state signatures (top panels) and the leading Standard Model background $pp \rightarrow Z + \text{jets}$ (lower panels). We explore the correlations between the leading and subleading jet transverse momenta (left) and the missing transverse energy vs the invariant mass of the leading dijet system (right).

B. Data

After establishing the NLO description of leptogluon pair production and studying the main kinematic features of the signal and background we are now ready to compare the precision predictions to LHC data. Specifically, we rely on the leptoquark searches by CMS [46]. Leptoquarks (lq) are described by a minimal extension of the Standard Model including one additional color triplet scalar. Our discussion henceforth will cover charged leptogluons only. The event samples for the signal are originally generated using PYTHIA 6.422 for a range of leptoquark masses $m_{lq} = 250 - 900$ GeV, with a central renormalization and factorization scale $\mu = m_{lq}$. The major backgrounds are determined either from control samples in data or from Monte Carlo simulations normalized to data in selected control regions. The available experimental data corresponds to the $\sqrt{S} = 7$ TeV run with 5 fb^{-1} of integrated luminosity.

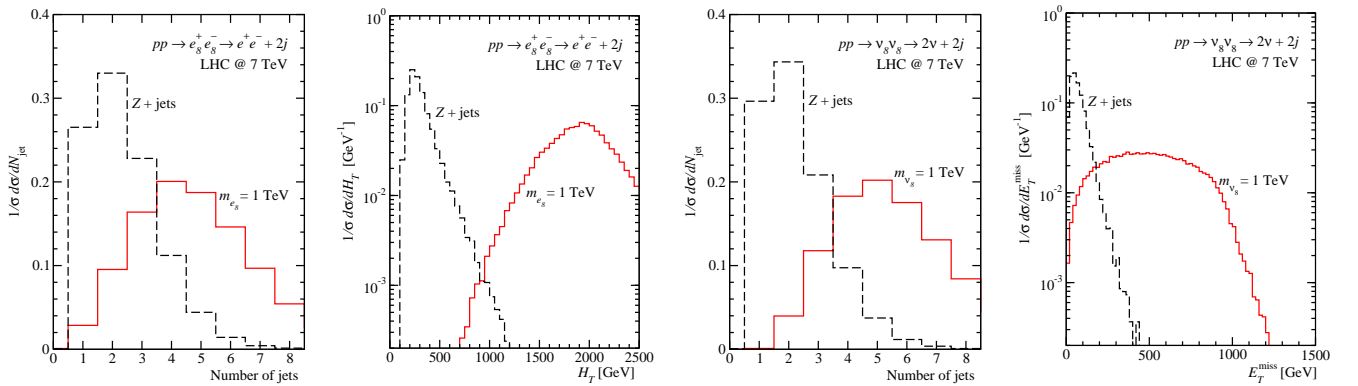


Figure 15: Differential cross sections as a function of the jet multiplicity and the total visible (resp. missing) transverse energy for charged (left panels) and neutral (right panels) leptogluons. We also include the leading background $pp \rightarrow Z + \text{jets}$. All the histograms we normalize to unity.

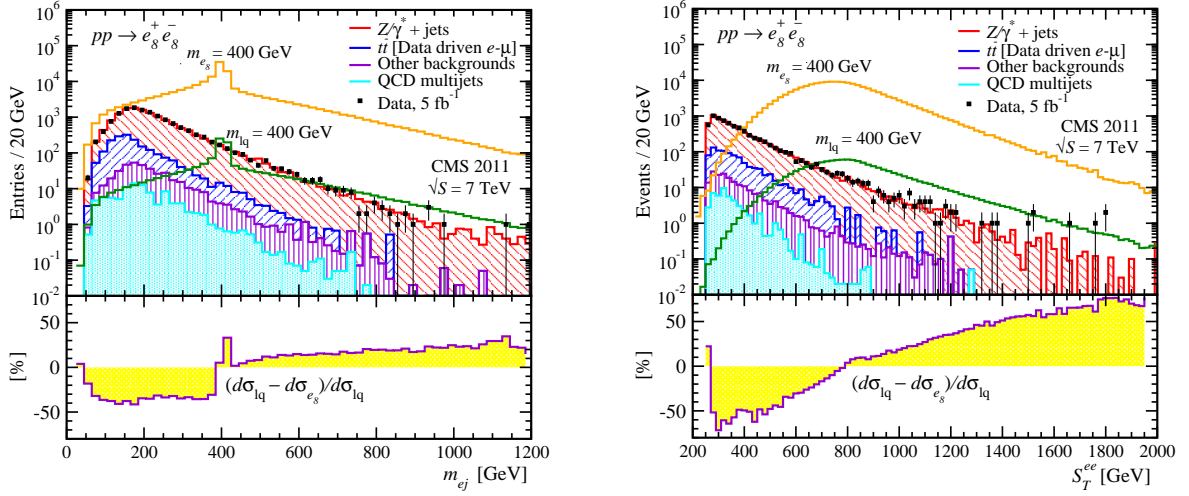


Figure 16: Distributions for the lepton-jet invariant mass (left) and the scalar transverse energy (right) for leptogluon pair production followed a decay into a lepton and a jet. The backgrounds we display as cumulative histograms and are taken from [46, 53]. The leptogluon signal is reweighted to the NLO prediction. For comparison, we also include the leptoquark signal for the same mass. The bottom panels illustrate the relative differences between the leptogluon and leptoquark distributions.

For further details we refer the reader to Ref. [46].

We now replace the leptoquark signal in the CMS leptoquark search with simulated leptogluon events, reweighted to the NLO rate for each assumed leptogluon mass. Following Ref. [46], we model the triggers by a set of initial acceptance cuts. They are tailored to select potential e^+e^-jj candidates among those events with two hard central leptons and QCD jets. Moreover, the jets are required to have a spatial separation of with respect to the electron candidates, while the dilepton invariant mass is enforced to fulfill

$$\begin{aligned} p_T(e) &> 40 \text{ GeV} & |\eta_e| &< 2.5 & m(e^+e^-) &> 60 \text{ GeV} & S_T^{ee} &> 250 \text{ GeV} \\ p_T(j) &> 30 \text{ GeV} & |\eta_j| &< 2.4 & \Delta R_{ej} &> 0.3. \end{aligned} \quad (8)$$

The cut on the scalar transverse energy $S_T^{ee} = p_T(e^+) + p_T(e^-) + p_T(j_1) + p_T(j_2)$ significantly reduces the combinatorial backgrounds.

After this selection the data is well compliant with the Standard Model background expectations, as reflected in Figures 16 and 17. Figure 16 shows the electron-jet invariant mass m_{ej} (left) and the scalar transverse energy S_T^{ee} (right) after acceptance cuts. Data we display as black circles while the backgrounds form cumulative histograms and are taken from [46, 53]. Finally, we overlay the leptogluon and leptoquark signals (solid lines), normalized to the respective NLO rates [54]. The masses of both resonances we fix to $m = 400 \text{ GeV}$, to provide a replica of Figure 2 from Ref. [46] including the leptogluon pair signal. In the lower panels we show the relative bin-by-bin differences between the leptoquark and the leptogluon predictions for identical masses. To deal with combinatorial issues when reconstructing the leptogluon mass, we distinguish two kinematic regions $\phi \in [0, \pm\pi]$ and we pair each of the leptons within a given event to the highest p_T jet of the same hemisphere.

Adopting the leptoquark analysis we can derive an approximate leptogluon mass. Our starting point is the acceptance–reconstruction efficiency factor as a function of the leptoquark mass, provided by CMS [53]. This we combine with the leptoquark acceptances to get the corresponding mass-dependent efficiencies ϵ_{lq} . The acceptances we estimate resorting to a leptoquark simulation within MADGRAPH5 and implementing the cuts in Eq.(8). The same strategy we follow to evaluate the corresponding leptogluon acceptances. Finally, we assume that the leptoquark efficiencies ϵ_{lq} can be exported to leptoglons, $\epsilon_{lq} \simeq \epsilon_{e8}$, and derive the combined acceptance–reconstruction efficiency factors for leptoglons as a function of m_{e8} .

We observe that the discrepancies between the leptoquark and leptogluon acceptances, and so on the resulting acceptance–efficiency factors, are indeed small. In spite of the intrinsically distinct kinematics of color–triplet scalars vs color–octet fermions, non-negligible differences arise primarily in phase space regions hardly passing the cuts of Eq.(8). They mostly attain tails in the transverse momentum and rapidity distributions. We study these differences for a number of representative distributions and find them typically at the $\mathcal{O}(10)\%$ level. This is also indicative that $\epsilon_{lq} \simeq \epsilon_{e8}$ is a reasonable hypothesis.

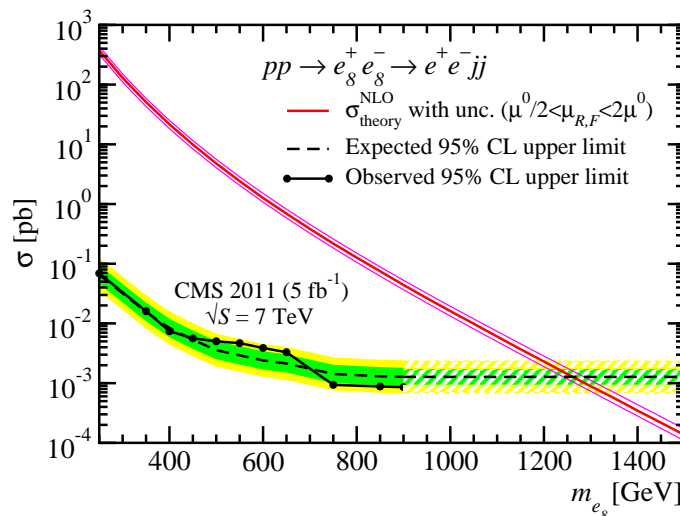


Figure 17: Expected and observed 95% CL limits on leptogluon pair production, followed by a decay into a lepton and a jet, based on the CMS leptoquark searches [46, 53]. The uncertainty bands represent 68% and 95% CL. We overlay the predicted production rates to NLO, including the theoretical uncertainty estimated from a full scale variation.

Finally, we take the CMS leptoquark limits from a modified frequentist confidence level (CL) analysis [55] and translate them into the leptogluon limit, extending them to leptogluon masses $m_{e_8} = 900 \text{ GeV} - 1.5 \text{ TeV}$. This procedure is valid so long as the reconstruction efficiency does not change significantly within this mass range. This assumption is justified given the rather general analysis strategy and the experimental setup [53].

In Figure 17 we show the expected and observed 95% CL upper limits on the rate for charged leptogluon pair production as a function of the mass. The uncertainty bands around the median expected limits correspond to 1 and 2σ . We overlay a two-sided magenta band accounting for the theoretical uncertainties using the NLO predictions, derived from the independent variation of the renormalization and factorization scales around the central value, $\mu^0/2 < \mu < 2\mu^0$. The intersection of the expected and the predicted rates defines a 2σ exclusion of $m_{e_8} \lesssim 1.2 - 1.3 \text{ TeV}$. This result constitutes a major improvement of the leptogluon mass bounds quoted at present [17].

IV. SUMMARY

We have studied the pair production of color-octet leptons at the LHC. These leptogluons constitute a minimal extension of the Standard Model by charged e_8^\pm and neutral ν_8 fields coupling to quarks and leptons via higher-dimensional operators.

In the first part of the paper we have reported on the complete NLO calculation of the LHC production rate, using MADGOLEM. The genuine new physics structures like Catani–Seymour dipoles and field as well as mass renormalization are part of the automated setup. We find large production rates around $\mathcal{O}(10) \text{ fb}$ for $\sqrt{S} = 8 \text{ TeV}$ and leptogluon masses in the TeV range. Significant quantum corrections arise mostly from pure QCD, *i.e.* virtual gluons and the massless initial/final state radiation. Leptogluon-mediated effects are mass-suppressed. The remaining theoretical uncertainty reduces from $\sim 65\%$ at LO down to $\sim 30\%$ at NLO. The NLO predictions are stable across the relevant phase space regions and agree well with results using LO multi-jet merging. This allows us to re-weight event simulations using jet merging to the NLO total cross section.

In the second part we have studied LHC signatures of leptogluon pair production. We have described the leptogluon couplings to matter fields in terms of a dimension 5, generation-diagonal $l_s l g$ chromomagnetic interaction. Leptogluon pairs appear as characteristic dijet plus dilepton signatures, featuring hard transverse momenta and large invariant masses. These quantities can easily be distinguished from the irreducible background, mainly governed by $pp \rightarrow Z + \text{jets}$. For charged leptogluons, the signature is the same to leptoquarks.

Finally, we use this fact to promote the current CMS leptoquark searches to leptogluon searches. We exclude the existence of charged leptogluons in the above framework with masses below $\sim 1.2 - 1.3 \text{ TeV}$.

Aside from its phenomenological relevance our work shows how the automated MADGOLEM framework can be used to efficiently study new physics models at the LHC. It completely automatizes the calculation of NLO cross sections

and distributions for pair production of new particles. MADGOLEM is an independent modular add-on to MADGRAPH and can easily be interfaced with its multiple user options and analysis tools. Following the present final testing phase we will make the code available to the theoretical and experimental communities at the LHC.

Acknowledgments

The work presented here has been in part supported by the Concerted Research action “Supersymmetric Models and their Signatures at the Large Hadron Collider” and the Strategic Research Program “High Energy Physics” of the Vrije Universiteit Brussel (VUB) and by the Belgian Federal Science Policy Office through the Interuniversity Attraction Pole IAP VI/11. DG acknowledges support by the International Max Planck Research School for Precision Tests of Fundamental Symmetries. It is our pleasure to deeply thank our CMS experimental colleagues, very specially the CMS group at VUB, for plenty of enlightening discussions and for providing us with the experimental data and the background simulation displayed in Figures 16 and 17.

Appendix: renormalization

Basic setup The ultraviolet renormalization counter terms we generate automatically from the QGRAF leading-order amplitude. The respective field, mass and g_s renormalization constants we conventionally phrase in terms of two-point functions. They are part of the leptogluon model implementation and supplied as a separate library. At present, MADGOLEM fully supports the calculation of NLO QCD corrections for the Standard Model, the MSSM and several other extensions of the Standard Model featuring heavy colored resonances (e.g. sgluons). All the necessary renormalization constants we define through the relation between the bare and the renormalized fields, masses and couplings – the former being denoted with a “0” superscript:

$$\Psi^{(0)} \rightarrow Z_\Psi^{1/2} \Psi \quad m_\Psi^{(0)} \rightarrow m_\Psi + \delta m_\Psi \quad g_s^{(0)} \rightarrow g_s + \delta g_s, \quad (9)$$

where Ψ stands for all the strongly interacting degrees of freedom of the model, in our case $\Psi = q, g, l_s$.

Given a generic QCD interaction with Lagrangian density $\mathcal{L}(\Psi, m_\Psi, g_s)$, we define its associated counterterm $\delta \mathcal{L}(\Psi, m_\Psi, g_s, \delta \Psi, \delta m_\Psi, \delta g_s)$ as

$$\mathcal{L}(\Psi^{(0)}, m_\Psi^{(0)}, g_s^{(0)}) = \mathcal{L}(\Psi, m_\Psi, g_s) + \delta \mathcal{L}(\Psi, m_\Psi, g_s, \delta \Psi, \delta m_\Psi, \delta g_s). \quad (10)$$

For further details on our notation setup, we refer the reader to Appendix D of Ref. [22].

Renormalization of the strong coupling constant In the presence of the leptogluon field, the β -function of the Standard Model, and thereby the strong coupling constant renormalization, get modified. Using standard notation, we may formally express the quantum corrections to the quark-gluon ($q\bar{q}g$) vertex in terms of the gluon (Z_3) and quark (Z_2) field-strength renormalization constants:

$$Z_1 = Z_g Z_2 Z_3^{1/2}. \quad (11)$$

These factors we can expand to order $\mathcal{O}(\alpha_s)$ as $Z_i = 1 + \delta_i + \mathcal{O}(\alpha_s^2)$, with the counterterms δ_i being conventionally defined in the $\overline{\text{MS}}$ scheme. The strong coupling constant renormalization at one loop we can thus write as

$$\delta g_s = \delta_1 - \delta_2 - \frac{1}{2} \delta_3. \quad (12)$$

Leptogluons only couple to matter fields through higher-dimensional operators, such as the leptogluon-lepton-gluon interaction described by Eq.(5). Consequently, quark self-energies – and hence δ_2 – are not affected by the presence of the leptogluons. The fermionic contribution to the β function remains therefore unaltered with respect to that of the Standard Model:

$$\delta_2^{\overline{\text{MS}}} = -\frac{\alpha_s}{4\pi} C_F \Delta_\epsilon. \quad (13)$$

The shifted pole in the $\overline{\text{MS}}$ prescription is $\Delta \equiv \frac{1}{\epsilon} - \gamma_E + \log(4\pi)$. The same reason explains the absence of leptogluon-mediated corrections to the quark-gluon vertex at one-loop, which means that

$$\delta_1 = \delta_1^{\text{SM}} = -\frac{\alpha_s}{4\pi} (C_A + C_F) \Delta_\epsilon. \quad (14)$$

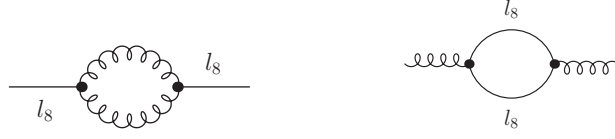


Figure 18: Feynman diagrams for the leptogluon field renormalization at $\mathcal{O}(\alpha_s)$ and for the leptogluon-mediated corrections to the gluon field renormalization at $\mathcal{O}(\alpha_s)$.

Instead, the pure QCD gluon/leptogluon interaction furnishes a novel piece to the gluon self-energies, as displayed in Figure 18. The latter results into

$$\delta_3^{l_s} = -s C_A \frac{\alpha_s}{3\pi} \Delta_\epsilon \quad (15)$$

with $s = 1(1/2)$ for $l_s = e_s^\pm(\nu_s)$. Adding up the above result to the Standard Model contribution we get

$$\delta_3^{\overline{\text{MS}}} = \delta_3^{\text{SM}} + \delta_3^{l_s} = \frac{\alpha_s}{4\pi} \left(\frac{5}{3} C_A - C_F N_F T_R \right) - s \frac{\alpha_s}{3\pi} C_A \Delta_\epsilon. \quad (16)$$

The final expression for δg_s we obtain by plugging Eqs.(14)-(16) back into Eq.(12), while explicitly decoupling the heavy (H) colored states – in our case, these are the top-quark and the leptogluon field(s). We implement such subtraction in a conventional zero-momentum scheme [23], as described in Ref. [35]. That way we leave the renormalization group running of α_s to be merely determined by the light (L) degrees of freedom. This corresponds to the definition of the measured value of the strong coupling, for example in a combined fit with the parton densities. The renormalization constant finally reads

$$\delta g_s = -\frac{\alpha_s}{4\pi} \frac{\beta_0^L + \beta_0^H}{2} \Delta_\epsilon - \frac{\alpha_s}{4\pi} \left[\frac{1}{3} \log \left(\frac{m_t^2}{\mu^2} \right) + 2s \frac{C_A}{3} \log \left(\frac{m_{l_s}^2}{\mu^2} \right) \right]. \quad (17)$$

Both light (L) and heavy (H) colored particles contribute to the coefficient of the beta function, which in our leptogluon model reads $\beta_0 = \beta_0^L + \beta_0^H$, with

$$\beta_0^L = \left[\frac{11}{3} C_A - C_F N_F T_R \right] \quad \text{and} \quad \beta_0^H = - \left[C_F T_R + 4s \frac{C_A}{3} \right]. \quad (18)$$

By default, MADGOLEM sets the number of active flavors to $N_F = 5$. Standard conventions for the $SU(3)_c$ color factors $C_F = 4/3$, $C_A = 3$ and $T_R = \frac{1}{2}$ are assumed throughout.

Renormalization of the leptogluon sector As a massive, color-adjoint particle, the leptogluon 2-point correlation function receives $\mathcal{O}(\alpha_s)$ corrections due to virtual gluon interchange, as shown in Figure 18. The corresponding UV divergences we can absorb into a redefinition of the leptogluon mass m_{l_s} and field-strength δZ_{l_s} . Both quantities we renormalize in the on-shell scheme. The renormalization conditions require i) the renormalized leptogluon mass to be the pole of the real part of the corresponding propagator; and ii) the renormalized propagator to have unit residue. These conditions we can cast in the following guise:

$$\Re \hat{\Sigma}_{l_s}(p^2 = m_{l_s}^2) = 0; \quad \lim_{p^2 \rightarrow m_{l_s}^2} \left[\frac{\not{p} + m_{l_s}}{p^2 - m_{l_s}^2} \right] \Re \hat{\Sigma}_{l_s}(p) \psi_{l_s}(p) = 0. \quad (19)$$

On the other hand, the (real part of the) renormalized leptogluon self-energy, $\Re \hat{\Sigma}_{l_s}$, we conventionally write as:

$$\Re \hat{\Sigma}_{l_s}(\not{p}) = \Re \left[\not{p} P_L \hat{\Sigma}_{l_s,L}(\not{p}) + \not{p} P_R \hat{\Sigma}_{l_s,R}(\not{p}) + m_{l_s} \Sigma_{l_s,S}(\not{p}) \right], \quad (20)$$

where the scalar components L, R and S render:

$$\hat{\Sigma}_{l_s,L/R}(\not{p}) = \Sigma_{l_s,L/R}(\not{p}) + \delta Z_{l_s,L/R} \quad (21)$$

$$\hat{\Sigma}_{l_s,S}(\not{p}) = \Sigma_{l_s,S}(\not{p}) - \frac{1}{2} (\delta Z_{l_s,L} + \delta Z_{l_s,R}) - \frac{\delta m_{l_s}}{m_{l_s}}. \quad (22)$$

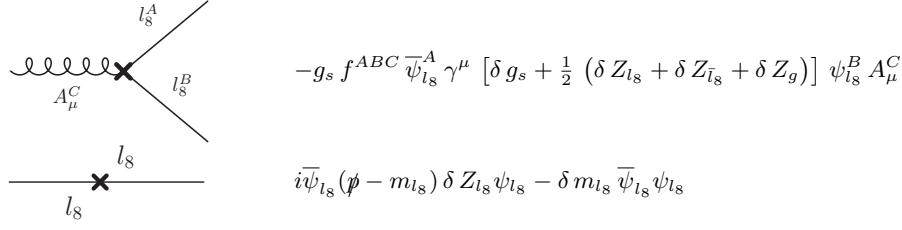


Table II: Counter term Feynman rules for the leptogluon-mediated interactions.

Enforcing the on-shell renormalization conditions Eq.(19) on the above leptogluon 2-point functions, we can finally anchor the field and mass renormalization constants as follows:

$$\begin{aligned} \delta Z_{l_s, L/R} &= -\Re \hat{\Sigma}_{l_s, L/R}(m_{l_s}^2) - m_{l_s}^2 \Re [\Sigma'_{l_s, L}(m_{l_s}^2) + \Sigma'_{l_s, R}(m_{l_s}^2) + 2 \Sigma'_{l_s, S}(m_{l_s}^2)] \\ \frac{\delta m_{l_s}}{m_{l_s}} &= \frac{1}{2} \Re [\Sigma_{l_s, L}(m_{l_s}^2) + \Sigma_{l_s, R}(m_{l_s}^2) + 2 \Sigma_{l_s, S}(m_{l_s}^2)]. \end{aligned} \quad (23)$$

Notice that the above expressions Eq.(20)-Eq.(23) equally hold for both charged and neutral leptogluon states. Moreover, as far as we disregard electroweak effects, in practice we will find no distinction between the respective left and right-handed components. The conventional shorthand notation $f'(p^2) \equiv df(p^2)/dp^2$ is employed therewith.

The analytic form of all renormalization constants we reduce down to 1 and 2-point scalar one-loop functions, in the conventions of [34]. UV divergences we handle by means of a standard 'tHooft-Veltman dimensional regularization scheme within $n = 4 - 2\epsilon$ dimensions. For the leptogluon mass and field strength renormalization, these quantities read:

$$\delta Z_{l_s} = -\frac{\alpha_s}{4\pi} C_A [\Re B_0(m_{l_s}^2, m_{l_s}^2, 0) - 4 m_{l_s}^2 \Re B'_0(m_{l_s}^2, m_{l_s}^2, 0) - 2] \quad (24)$$

$$\delta m_{l_s} = \frac{\alpha_s}{4\pi} C_A [2 - 3 \Re B_0(m_{l_s}^2, m_{l_s}^2, 0)]. \quad (25)$$

Unsurprisingly, the above expressions are identical to the gluon-mediated correction to the gluino field and mass renormalization constants. For the gluino case, however, we rely as well on the additional SUSY-QCD contributions triggered by the squark interchange.

Finally, the explicit analytical expressions for the different UV counter terms involving the leptogluon interactions $\delta \mathcal{L}$ we quote in Table II in terms of the field, mass and strong coupling renormalization constants.

-
- [1] L. Lyons, Prog. Part. Nucl. Phys. **10**, 227 (1983); H. Harari, Phys. Rept. **104**, 159 (1984).
 - [2] R. Aaij *et al.* [LHCb Collaboration], Phys. Rev. Lett. **110**, 021801 (2013) [arXiv:1211.2674 [hep-ex]].
 - [3] J. C. Pati and A. Salam, Phys. Rev. D **10**, 275 (1974) [Erratum-ibid. D **11**, 703 (1975)]; H. Terazawa, K. Akama and Y. Chikashige, Phys. Rev. D **15**, 480 (1977); M. A. Shupe, Phys. Lett. B **86**, 87 (1979).
 - [4] H. Fritzsch and G. Mandelbaum, Phys. Lett. B **102**, 319 (1981); H. Terazawa, Phys. Rev. D **22**, 184 (1980); H. Harari and N. Seiberg, Phys. Lett. B **98**, 269 (1981); R. Barbieri, R. N. Mohapatra and A. Masiero, Phys. Lett. B **105**, 369 (1981) [Erratum-ibid. B **107**, 455 (1981)]; O. W. Greenberg and J. Sucher, Phys. Lett. B **99**, 339 (1981).
 - [5] W. Buchmüller, R. Rückl and D. Wyler, Phys. Lett. B **191**, 442 (1987) [Erratum-ibid. B **448**, 320 (1999)].
 - [6] M. A. Luty and R. N. Mohapatra, Phys. Lett. B **396**, 161 (1997) [hep-ph/9611343].
 - [7] K. Agashe, R. Contino and A. Pomarol, Nucl. Phys. B **719**, 165 (2005) [hep-ph/0412089].
 - [8] M. Gabella, T. Gherghetta and J. Giedt, Phys. Rev. D **76**, 055001 (2007) [arXiv:0704.3571 [hep-ph]].
 - [9] M. R. Buckley and E. T. Neil, arXiv:1209.6054 [hep-ph].
 - [10] K. Hagiwara, D. Zeppenfeld and S. Komamiya, Z. Phys. C **29**, 115 (1985); V. D. Barger, K. Hagiwara, T. Han and D. Zeppenfeld, Phys. Lett. B **220**, 464 (1989); U. Baur, M. Spira and P. M. Zerwas, Phys. Rev. D **42**, 815 (1990).
 - [11] T. Han, I. Lewis and Z. Liu, JHEP **1012**, 085 (2010) [arXiv:1010.4309 [hep-ph]].
 - [12] H. Harari, Phys. Lett. B **156**, 250 (1985); S. F. King and S. R. Sharpe, Nucl. Phys. B **253**, 1 (1985); U. Baur and K. H. Streng, Phys. Lett. B **162**, 387 (1985); Y. Nir, Phys. Lett. B **164**, 395 (1985); K. H. Streng, Z. Phys. C **33**, 247 (1986); T. G. Rizzo, Phys. Rev. D **33**, 1852 (1986); Phys. Rev. D **34**, 133 (1986); J. L. Hewett and T. G. Rizzo, Phys. Rev. D **56**, 5709 (1997); A. Celikel, M. Kantar and S. Sultansoy, Phys. Lett. B **443**, 359 (1998); M. Sahin, S. Sultansoy and S. Turkoz, Phys. Lett. B **689**, 172 (2010); A. N. Akay, H. Karadeniz, M. Sahin and S. Sultansoy, Europhys. Lett. **95**, 31001 (2011) [arXiv:1012.0189 [hep-ph]]; J. L. Abelleira Fernández *et al.* [LHeC Study Group Collaboration], J. Phys. G **39**, 075001 (2012).

- [13] R. S. Chivukula, M. Golden and E. H. Simmons, Phys. Lett. B **257**, 403 (1991).
- [14] M. C. González-García and S. F. Novaes, Phys. Lett. B **389**, 707 (1996) [hep-ph/9609393].
- [15] T. Mandal and S. Mitra, arXiv:1211.6394 [hep-ph].
- [16] M. Sahin, arXiv:1302.5747 [hep-ph].
- [17] J. Beringer et al. (Particle Data Group), Phys. Rev. D **86**, 010001 (2012).
- [18] W. Bartel *et al.* [JADE Collaboration], Z. Phys. C **36**, 15 (1987).
- [19] D. López-Val, D. Gonçalves-Netto, K. Mawatari, T. Plehn and I. Wigmore, arXiv:1209.2797 [hep-ph].
- [20] T. Binoth, D. Gonçalves-Netto, D. López-Val, K. Mawatari, T. Plehn, and I. Wigmore, Phys. Rev. D **84**, 075005 (2011).
- [21] D. Gonçalves-Netto, D. López-Val, K. Mawatari, T. Plehn and I. Wigmore, Phys. Rev. D **85**, 114024 (2012).
- [22] D. Gonçalves-Netto, D. López-Val, K. Mawatari, T. Plehn and I. Wigmore, Phys. Rev. D **87**, 014002 (2013).
- [23] W. Beenakker, R. Höpker, M. Spira, and P. M. Zerwas, Phys. Rev. Lett. **74**, 2905 (1995); W. Beenakker, R. Höpker, M. Spira and P. M. Zerwas, Nucl. Phys. B **492**, 51 (1997).
- [24] W. Beenakker, M. Krämer, T. Plehn, M. Spira and P. M. Zerwas, Nucl. Phys. B **515**, 3 (1998).
- [25] J. Pumplin, D. R. Stump, J. Huston, H. L. Lai, P. Nadolsky, and W. K. Tung, JHEP **0207**, 012 (2002).
- [26] W. Beenakker, R. Höpker, M. Spira and P. M. Zerwas, Z. Phys. C **69**, 163 (1995) [hep-ph/9505416].
- [27] S. Catani and M. H. Seymour, Phys. Lett. B **378**, 287 (1996); S. Catani and M. H. Seymour, Nucl. Phys. B **485**, 291 (1997) [Erratum-ibid. B **510**, 503 (1998)].
- [28] S. Catani, S. Dittmaier, M. H. Seymour and Z. Trocsanyi, Nucl. Phys. B **627**, 189 (2002).
- [29] R. Frederix, T. Gehrmann, and N. Greiner, JHEP **0809**, 122 (2008); and JHEP **1006**, 086 (2010).
- [30] S. Frixione, Z. Kunszt, and A. Signer, Nucl. Phys. B **467**, 399 (1996); Z. Nagy and Z. Trocsanyi, Phys. Rev. D **59**, 014020 (1999) [Erratum-ibid. D **62**, 099902 (2000)].
- [31] P. Nogueira, J. Comput. Phys. **105**, 279 (1993).
- [32] G. Cullen, N. Greiner, A. Guffanti, J. -P. Guillet, G. Heinrich, S. Karg, N. Kauer and T. Kleinschmidt *et al.*, Nucl. Phys. Proc. Suppl. **205-206**, 67 (2010); N. Greiner, A. Guffanti, T. Reiter and J. Reuter, Phys. Rev. Lett. **107**, 102002 (2011).
- [33] T. Binoth, J. P. Guillet, G. Heinrich, E. Pilon, and T. Reiter, Comput. Phys. Commun. **180**, 2317 (2009); G. Cullen, J. P. Guillet, G. Heinrich, T. Kleinschmidt, E. Pilon, T. Reiter and M. Rodgers, Comput. Phys. Commun. **182**, 2276 (2011).
- [34] A. van Hameren, Comput. Phys. Commun. **182**, 2427 (2011).
- [35] J. C. Collins, F. Wilczek, and A. Zee, Phys. Rev. D **18**, 242 (1978); S. Berge, W. Hollik, W. M. Mösele, and D. Wackeroth, Phys. Rev. D **76**, 034016 (2007).
- [36] T. Hahn, Comput. Phys. Commun. **140**, 418 (2001); T. Hahn and M. Pérez-Victoria, Comput. Phys. Commun. **118**, 153 (1999); T. Hahn and C. Schappacher, Comput. Phys. Commun. **143**, 54 (2002); T. Hahn and M. Rauch, Nucl. Phys. Proc. Suppl. **157**, 236 (2006).
- [37] A. Sommerfeld, Ann. der Phys. **403**, 257 (1931).
- [38] W. Beenakker, S. Brensing, M. Krämer, A. Kulesza, E. Laenen and I. Niessen, JHEP **0912**, 041 (2009); J. Debove, B. Fuks and M. Klasen, Nucl. Phys. B **849**, 64 (2011); A. Kulesza and L. Motyka, Phys. Rev. Lett. **102**, 111802 (2009); A. Kulesza and L. Motyka, Phys. Rev. D **80**, 095004 (2009); M. Beneke, P. Falgari and C. Schwinn, Nucl. Phys. B **842**, 414 (2011); P. Falgari, C. Schwinn and C. Wever, JHEP **1206**, 052 (2012); M. R. Kauth, J. H. Kühn, P. Marquard and M. Steinhauser, Nucl. Phys. B **857**, 28 (2012).
- [39] T. Plehn, D. Rainwater, and P. Skands, Phys. Lett. B **645**, 217 (2007).
- [40] J. Alwall, S. de Visscher, F. Maltoni, JHEP **0902**, 017 (2009).
- [41] M. L. Mangano, M. Moretti, and R. Pittau, Nucl. Phys. B **632**, 343 (2002).
- [42] for a pedagogical introduction see e.g. T. Plehn, Lect. Notes Phys. **844**, 1 (2012) [arXiv:0910.4182 [hep-ph]].
- [43] J. Alwall, M. Herquet, F. Maltoni, O. Mattelaer and T. Stelzer, JHEP **1106**, 128 (2011).
- [44] T. Sjöstrand, S. Mrenna and P. Z. Skands, JHEP **0605**, 026 (2006).
- [45] H. Dreiner, M. Krämer and J. Tattersall, arXiv:1211.4981 [hep-ph].
- [46] S. Chatrchyan *et al.* [CMS Collaboration], Phys. Rev. D **86**, 052013 (2012).
- [47] S. Ambrosanio, G. L. Kane, G. D. Kribs, S. P. Martin and S. Mrenna, Phys. Rev. D **54**, 5395 (1996).
- [48] P. de Aquino, F. Maltoni, K. Mawatari and B. Oexl, JHEP **1210**, 008 (2012).
- [49] N. D. Christensen and C. Duhr, Comput. Phys. Commun. **180**, 1614 (2009); C. Duhr and B. Fuks, Comput. Phys. Commun. **182**, 2404 (2011).
- [50] C. Degrande, C. Duhr, B. Fuks, D. Grellscheid, O. Mattelaer and T. Reiter, Comput. Phys. Commun. **183**, 1201 (2012); P. de Aquino, W. Link, F. Maltoni, O. Mattelaer and T. Stelzer, Comput. Phys. Commun. **183**, 2254 (2012).
- [51] E. Conte, B. Fuks and G. Serret, Comput. Phys. Commun. **184**, 222 (2013).
- [52] C. Englert, T. Plehn, P. Schichtel and S. Schumann, Phys. Rev. D **83**, 095009 (2011).
- [53] CMS Collaboration, private correspondence.
- [54] M. Krämer, T. Plehn, M. Spira and P. M. Zerwas, Phys. Rev. D **71**, 057503 (2005).
- [55] T. Junk, Nucl. Instrum. Meth. A **434**, 435 (1999) [hep-ex/9902006]; A. L. Read, CERN-OPEN 2000-205 (2000).